Spherical Mean Diffusion-Weighted MRI Reveals Peripheral Axonal Integrity Following Trauma-Induced Wallerian Degeneration

Kelvin Chen[1, 2]; Thammathida Ketsiri, Ph.D.[1]; Richard D. Dortch, Ph.D.[1]

[1]Department of Translational Neuroscience, Barrow Neurological Institute, Phoenix, AZ, USA; [2]University of Virginia, Charlottesville, VA, USA

ABSTRACT

Tissue-specific indices rendered by the spherical mean technique (SMT) when applied to multi-compartmental diffusion MRI models enable the systematic profiling of the pathophysiological characteristics of traumatic peripheral nerve injury (TPNI), including tissue microstructure, heterogeneity, and cellularity. Of note, the current clinical management of TPNI is complicated by challenges in assessing nerve injury severity and monitoring the success of post-operative nerve regeneration, thereby delaying clinical decision-making. Here we present a preclinical application of SMT to estimate axonal volume fraction (V_{ax}) and axonal diffusivity (D_{ax}) from computer simulations based on pathologically realistic voxelized tissue microgeometries. Following model validation and optimization, SMT-derived estimates displayed strong agreements with experimental data from histology and diffusion MRI. SMT-based diffusion biomarkers thus offer improved pathological specificity and sensitivity to nerve re/degeneration relative to conventional MRI methods (e.g., DTI, DKI, MRN), which effectively moves SMT toward clinical trial readiness given its clinical utility in warranting surgical interventions by physicians when failed nerve repairs are identified.

INTRODUCTION

Peripheral nerves that incur trauma will undergo axonal loss, demyelination, and Schwann cell denervation distal to the infarcted site followed by muscle atrophy, sensorimotor dysfunction, neuroma formation, etc. prior to reinnervation.[1]

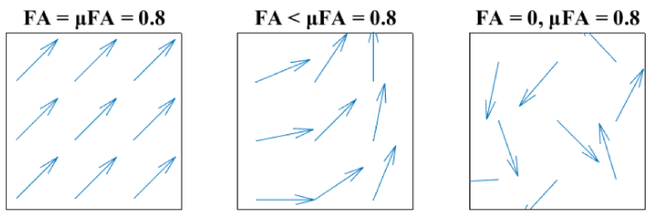

Figure 1. The degree of anisotropy reflects the directional architecture of water protons (denoted by the arrows) in a diffusion process. Microscopic parameters are confounded by complex, arbitrary neurite orientation distributions (single orientation, left; fiber dispersion, middle; uniform distribution, right) resulting from fiber crossings, orientation dispersion, and axon undulation. Such effects are minimal in SMT, however, for it is an orientation-invariant method by which diffusion signals are powder averaged across all gradient directions using only $\geq$ two b-shells.[2, 3]

METHODS

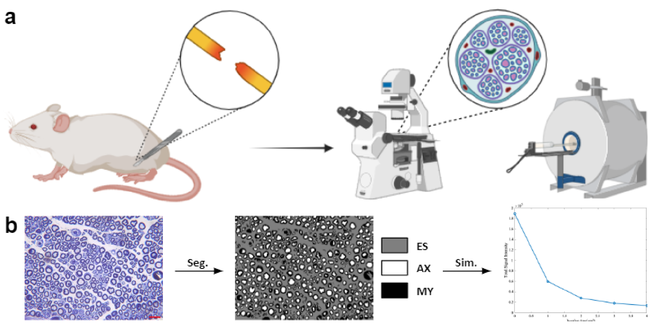

Figure 2. Distal sciatic nerves were harvested from rat models of TPNI and categorized by injury type (sham, crush, cut/repair) and post-operative time point (1, 2, 4, 12 weeks) (a). Toluidine blue-stained histology images (scale bar: 20 μm) from light microscopy and MRI were semantically segmented into three compartments (extra-axonal, ES; intra-axonal, AX; myelin/debris, MY) followed by simulating the diffusion signals via the finite difference method with SMT fitting (b).

Generalized SMT Model Assumptions[3]:

- Myelin signals are excluded due to a rapid T_2 relaxation while the T_2s of extra- and intra-axonal spaces are homogeneous.
- Axial diffusivities along the axonal fibers are the same wherein $D_{ax} = D_{\parallel}^{ext} = D_{\parallel}^{int}$ due to the lack of restriction per axon.
- The first-order tortuosity limit is true such that $D_{\perp}^{ext} = (1-V_{ax})D_{ax}$ and $D_{\perp}^{int} \approx 0$ due to minuscule axon diameters (1–2 μm).

SMT Modeling. The spherical mean diffusion signal $\bar{S}$ was derived from isolated mean extra- and intra-axonal signals to approximate the parameters $V_{ax} \in [0, 1]$ and $D_{ax} \in [0, D_{ax}^{free}]$, where $D_{ax}^{free} \approx 1.88$ μm^2/ms at 17 °C for ex vivo rodent models.[2]

$$\underbrace{h_b(g,\omega \mid V_{ax}, D_{ax}) = V_{ax}h_b^{int}(g,\omega) + (1-V_{ax})h_b^{ext}(g,\omega)}_{\text{Multi-compartment microscopic diffusion model}} \xrightarrow{\text{SMT}} \underbrace{\bar{S} = V_{ax}\bar{S}_{int} + (1-V_{ax})\bar{S}_{ext}}_{\text{Mean diffusion signal model}} \quad (1)$$

Attenuated diffusion signals due to Gaussian and non-Gaussian water diffusion were quantified by ADC and kurtosis, respectively.[4]

$$\underbrace{S(b) = S_0 \exp(-b\bar{D})}_{\text{Stejskal-Tanner equation}} \xrightarrow{\text{Cumulant expansion}} \underbrace{S(b) = S_0 \exp\left(-b\bar{D} + \frac{1}{6}b^2\bar{D}^2\bar{K} + O(b^3)\right)}_{\text{Standard DKI signal representation}} \quad (2)$$

Diffusion MRI Signal Simulation & Analysis. Simulations were performed in 3D geometry (sphere) with restricted diffusion in silico in MATLAB with the MATI (Microstructural Analysis of Tissues by Imaging) package. Results were compared against their corresponding ground truth values to test model assumptions and the precision and accuracy of optimized SMT parameters.

RESULTS & DISCUSSION

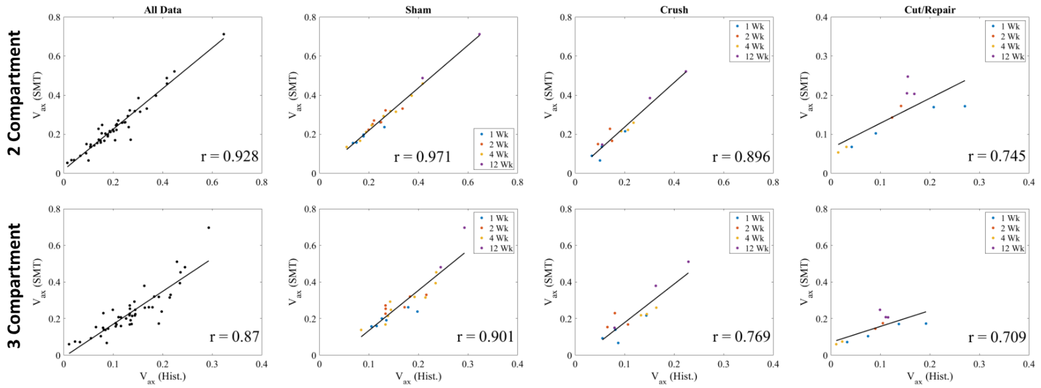

Figure 3. Correlation between SMT- and histology-derived V_{ax} was shown to be significantly linear for each injury type across all post-operative time points.

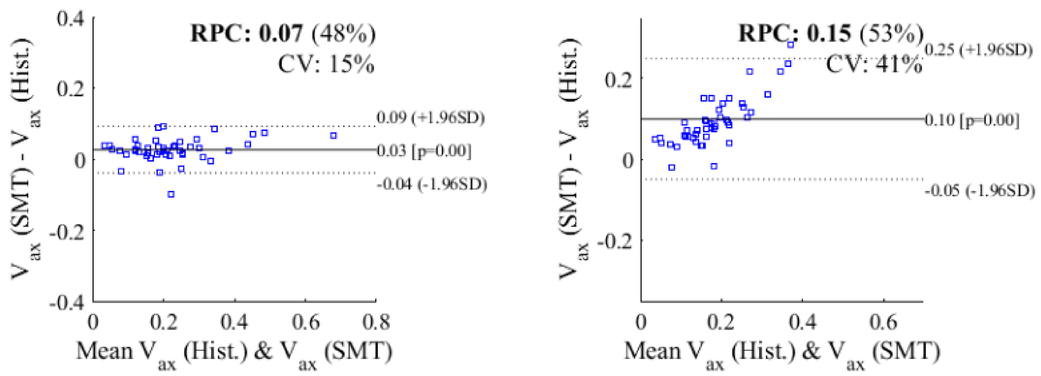

Figure 4. In comparison to the three-compartment model (right), a stronger agreement was observed in the two-compartment model (left) with higher repeatability and lower variability relative to the mean as shown in the Bland-Altman plots.

Harvest & Type	V_{ax} (Histology)	V_{ax} (SMT)																	
		G (mT/m)			Δ (ms)			δ (ms)			TE (ms)			b (ms/μm²)			τ (ms)		
		35	40	45	10	20	30	15	30	45	25	50	100	{0, 0.8, 1.6, 2.4, 3.2}	{0, 1, 2, 3, 4}	{0, 1.2, 2.4, 3.6, 4.8}	0.6	0.9	1.2
1 wk, Sham	0.246	0.261	0.261	0.261	0.240	0.260	0.266	0.192	0.259	0.265	0.261	0.261	0.261	0.275	0.261	0.246	0.261	0.261	0.260
1 wk, Crush	0.202	0.215	0.215	0.215	0.201	0.215	0.217	0.168	0.215	0.214	0.215	0.217	0.215	0.225	0.215	0.205	0.215	0.215	0.215
1 wk, Cut/Repair	0.091	0.102	0.102	0.102	0.094	0.102	0.105	0.073	0.102	0.105	0.102	0.102	0.102	0.109	0.102	0.096	0.102	0.102	0.102

Harvest & Type	MD (μm²/ms)	D_{ax} (SMT)																	
		G (mT/m)			Δ (ms)			δ (ms)			TE (ms)			b (ms/μm²)			τ (ms)		
		35	40	45	10	20	30	15	30	45	25	50	100	{0, 0.8, 1.6, 2.4, 3.2}	{0, 1, 2, 3, 4}	{0, 1.2, 2.4, 3.6, 4.8}	0.6	0.9	1.2
1 wk, Sham	0.842	1.726	1.726	1.726	1.686	1.724	1.733	2.494	1.724	1.727	1.726	1.726	1.726	1.788	1.726	1.663	1.724	1.726	1.724
1 wk, Crush	0.763	1.736	1.736	1.736	1.711	1.735	1.734	2.622	1.736	1.721	1.736	1.734	1.736	1.779	1.736	1.690	1.734	1.736	1.734
1 wk, Cut/Repair	0.950	1.739	1.739	1.739	1.732	1.739	1.736	2.740	1.740	1.729	1.739	1.739	1.739	1.772	1.739	1.704	1.736	1.739	1.737

Table 1. Impact of varied pulsed gradient spin echo (PGSE) sequence parameters on V_{ax} (a) and D_{ax} (b) approximations in the SMT-based diffusion model. Errors in SMT-derived V_{ax}/D_{ax} estimates were observed to decrease with decreasing gradient separation and increasing gradient duration and b-value.

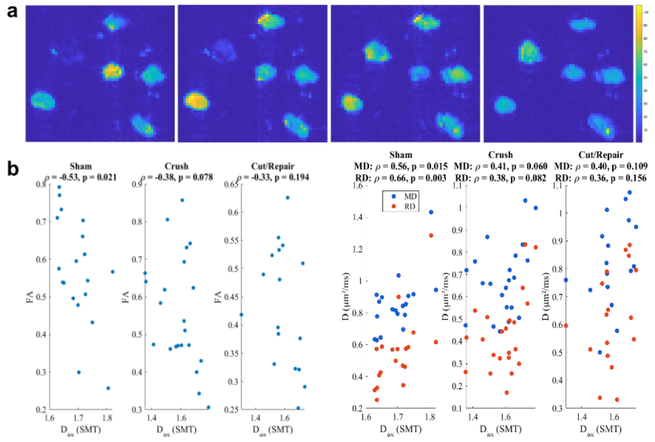

Figure 5. Representative distal DTI/DKI parameter maps based on diffusion data; note the nerve degeneration as shown by the elevated diffusivities and reduced FA followed by a partial nerve regeneration (a). A statistically significant relationship ($p \leq 0.05$) was not observed between SMT-derived D_{ax} and FA, MD, and RD (b); values outside of the bound $0 \leq D_{ax} \leq D_{ax}^{free}$ were removed.

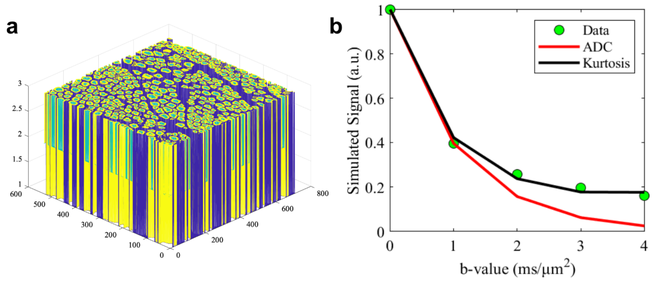

Figure 6. 3D meshes were reconstructed from 2D computational models whereby five image slices were taken to calculate the powder averaged signal from simulation (a). Signal attenuation due to non-Gaussian diffusivities is illustrated by the signal decay as a function of b-values (b).

CONCLUSION & FUTURE DIRECTIONS

SMT yielded tissue-specific indices that correlated strongly against histology and diffusion MRI data with reduced errors following SMT protocol optimization, which testify to the applicability of this technique in human clinical trials.

Limitations. Unlike white matter in the CNS, biased V_{ax} and/or D_{ax} estimates may result from the violation of certain SMT model assumptions, i.e. large peripheral axon diameters ($\leq$ 20 μm) and heterogeneous compartmental T_2s.

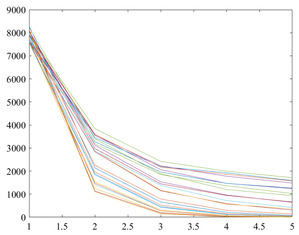

SNR = 30	V_{ax}	D_{ax} (μm²/ms)
Histology	0.202	-
Noise-free	0.217	1.731
Rician noise$_1$	0.213	1.687
Rician noise$_2$	0.209	1.697
⋮		
Rician noise$_n$	$(V_{ax})_n$	$(D_{ax})_n$

Figure 7. The noise regime of the simulated diffusion signals will follow a random Rician distribution.

ACKNOWLEDGEMENTS & REFERENCES

This work was supported by NIH grant R61NS127268 and the Barrow Neurological Foundation. KC thank TK and RDD for their dedicated mentorship and stimulating discussion throughout the course of this work.

1. Xu, S., Ito, A. (2023). *Current Opinion in Biomedical Engineering*, 100515.
2. Kaden, E., Kelm, N. D., Carson, R. P., Does, M. D., Alexander, D. C. (2016). *NeuroImage*, 139, 346-359.
3. Devan, S. P., Jiang, X., Bagnato, F., Xu, J. (2020). *Magnetic Resonance Imaging*, 74, 56-63.
4. Yablonskiy, D. A., Sukstanskii, A. L. (2010). *NMR in Biomedicine*, 23(7), 661-681.